Quantum-Mechanical ab Initio Simulation of the Raman and IR Spectra of $Fe_3Al_2Si_3O_{12}$ Almandine

A. M. Ferrari,*,† L. Valenzano,† A. Meyer,† R. Orlando,‡ and R. Dovesi†

Dipartimento di Chimica IFM and NIS (Nanostructured Interfaces and Surfaces) Centre of Excellence, Università di Torino, Via P. Giuria 7, 10125 Torino, Italy, and Dipartimento di Scienze e Tecnologie Avanzate, Università del Piemonte Orientale, Viale T. Michel 11, 15121 Alessandria, Italy

Received: March 4, 2009; Revised Manuscript Received: August 20, 2009

The IR and Raman spectra of the $Fe_3Al_2Si_3O_{12}$ almandine garnet were simulated using the periodic CRYSTAL code with an all-electron Gaussian-type basis set and the hybrid B3LYP functional. The wavenumbers of the 25 Raman-active modes (3 of A_{1g}, 8 of E_g, and 14 of F_{2g} symmetry) and 34 F_{1u} IR-active modes (17 TO and 17 LO) were computed, as were the IR intensities. Calculated wavenumbers are in excellent agreement with the various sets of experimental results, with the mean absolute difference $|\bar{\Delta}|$ being between 4 and 8 cm^{-1}. Graphical animation, available on the CRYSTAL Web site, provides a very comprehendible description of the movement of atoms and groups in each vibrational mode. The simulated reflectivity spectrum, obtained using a classical dispersion relation, is in excellent agreement with the measured one.

I. Introduction

Garnets, $X^{II}_3Y^{III}_2Si_3O_{12}$, are important rock-forming silicates, as major constituents of Earth's upper mantle and relevant phases of high-pressure metamorphic rocks in Earth's crust.[1] Almandine $Fe_3Al_2Si_3O_{12}$ is one of the most common members of the family and is usually found in garnet schists (a type of metamorphic rock composed mostly of mica). Almandine is used as a gemstone and as garnet paper, an important abrasive.

The building blocks are SiO_4 tetrahedra sharing corners with AlO_6 octahedra, with Fe^{2+} cations in dodecahedral coordination.

In the past decade, quantum mechanical calculations have been shown to be capable of accurately predicting the equilibrium geometries and vibrational frequencies of crystalline compounds. Garnets, because of their large unit cells, high symmetry, and available experimental data, represent challenging tests for modern periodic quantum mechanical codes.

In the present work, we have performed a complete vibrational analysis of almandine, including the Raman spectrum and the transverse optical (TO) and longitudinal optical (LO) parts of the infrared (IR) spectrum. The full set of wavenumbers (IR-active, Raman-active, and silent) has been generated, along with the IR intensities (work is in progress for the implementation of the tools that permit the computation of Raman intensities), using the ab initio quantum-mechanical periodic code CRYSTAL,[2] which has already been used for studies concerning the spectroscopic properties of other garnets.[3−6] The calculated results have also been compared with the most recent experimental data.[7−10]

For the first time with respect to our previous studies, the calculated IR intensities are compared with the experimental values, and the simulated reflectivity spectrum is directly compared with the corresponding experimental one.

To the authors' knowledge, this is the first ab initio study of the vibrational spectra of almandine. About 6 years ago, Gramaccioli and Pilati[11] published a similar investigation that was, however, based on a rigid-ion lattice-dynamical model whose parameters were determined by a best fit to a set of experimental data.

The movement of each atom for each mode is represented graphically by animations available on the Web, so that the reader can directly interpret the nature of the mode (stretching, bending, rotation of the tetrahedra, translation of the X cation, etc.), by simply looking at the animation. This article is organized as follows: The computational method is reported in section II, and in section III, the results are presented and discussed.

II. Computational Methods

Calculations were performed with the CRYSTAL06 code.[2] The hybrid B3LYP functional,[12,13] which has been shown to reproduce equilibrium geometries and vibrational frequencies[3,4,6,14−16] in excellent agreement with experimental data, was employed.

The level of accuracy in evaluating the Coulomb and Hartree−Fock exchange series is controlled by five parameters[2] that have been set to values of 8, 8, 8, 8, and 18. The reciprocal space was sampled according to a regular sublattice with a shrinking factor[2] equal to 2 that corresponds to three independent **k** vectors in the irreducible part of the Brillouin zone. The density functional theory exchange-correlation contribution was evaluated by numerical integration over the unit cell volume. In CRYSTAL, radial and angular points of the grid are generated through Gauss−Legendre radial quadrature and Lebedev two-dimensional angular point distributions. In the present calculations, a (75,974) grid was used (XLGRID keyword in the CRYSTAL06 manual[2]), which corresponds to a pruned grid with 75 radial and 974 angular points; details about the grid generation, the number of points in reciprocal space, and their influence on the accuracy and cost of calculation can be found in refs 3 and 5.

The threshold on the self-consistent field (SCF) energy was set to 10^{-7} Ha. The presence of Fe^{2+} ions in a d^6 electron configuration and the low symmetry of the dodecahedral site make the SCF convergence much slower (300−400 cycles,

* To whom correspondence should be addressed. E-mail: anna.ferrari@unito.it.
† Università di Torino.
‡ Università del Piemonte Orientale.

10.1021/jp901993e CCC: $40.75 © 2009 American Chemical Society
Published on Web 09/29/2009

TABLE 1: Calculated and Experimental[20,21] Geometries of Almandine $Fe_3Al_2(SiO_4)_3$[a]

	calc	exp[b]
a	11.6466	11.512(1)
O_x	0.03592	0.03395(10)
O_y	0.04736	0.04943(11)
O_z	0.65275	0.65268(11)
Fe_1-O	2.2358	2.2198(1)
Fe_2-O	2.4141	2.3634(1)
Al−O	1.9032	1.8882(2)
Si−O	1.6492	1.6364(2)

[a] Lattice parameters (a) and distances (Z−O) are in angstroms; O_i, $i = x, y, z$, represents the fractional oxygen coordinates. [b] Numbers in parentheses represent the experimental uncertainty.

compared to 20−40) than in andradite (Fe^{3+} in octahedral position, d^5 configuration).

An all-electron basis set was used for all atoms. Oxygen, aluminum, silicon, and iron are described by (8s)−(411sp)−(1d), (8s)−(611sp)−(1d), (8s)−(6311sp)−(1d), and (8s)−(64111sp)−(411d) contractions, respectively, used as such or with small modifications from previous works.[3−5] The complete basis sets and details on the computational parameters can be found on the CRYSTAL Web site,[17] where input and output files used for the calculations are reported.

The calculation of the vibrational wavenumbers at the Γ point was performed within the harmonic approximation. For a detailed description of the method and details on computational aspects, see refs 5, 14, and 18.

Observed and calculated wavenumbers, ν_v, were compared through three global indices defined as

$$\begin{aligned} \overline{|\Delta|} &= M^{-1}\sum_{v=1}^{M}|\nu_v - \nu_v^{\mathrm{ref}}| \\ \bar{\Delta} &= M^{-1}\sum_{v=1}^{M}\nu_v - \nu_v^{\mathrm{ref}} \\ |\Delta_{\max}| &= \max(|\nu_v - \nu_v^{\mathrm{ref}}|) \quad v = 1, 2, ..., M \end{aligned} \tag{1}$$

where M is the number of data points in the set and $\bar{\Delta}$, $|\bar{\Delta}|$, and $|\Delta_{\max}|$ (all in cm^{-1}) are the average of the difference, the average of the absolute difference, and the maximum absolute difference between the sets, respectively.

III. Results

The garnet structure is highly symmetric: the space group is $Ia\bar{3}d$, and the point group is O_h, with 48 symmetry operators. The Fe, Al, and Si atoms are in dodecahedral (D_2), octahedral (S_6), and tetrahedral (S_4) special positions, respectively. The oxygen atoms are in general positions as reported in Table 1, documenting the quite good agreement between calculated and experimental geometries:[19−21] the lattice parameter is overestimated by about 1%, and the Fe−O, Si−O, and Al−O distances are overestimated by 0.02−0.05, 0.02, and 0.01 Å, respectively. It is worth recalling, however, that experiments are performed at 100 K and atomic positions are affected by a certain amount of dynamic disorder that depends on temperature, whereas the computations refer to 0 K.

The decomposition of the reducible representation built on the basis of the Cartesian coordinates of the atoms in the unit cell leads to the following symmetry assignment of the 240 normal modes (this analysis is performed automatically by the CRYSTAL code)

$$\begin{aligned} \Gamma_{\mathrm{total}} = {} & 3A_{1g} \oplus 5A_{2g} \oplus 8E_g \oplus 14F_{1g} \oplus 14F_{2g} \oplus \\ & 5A_{1u} \oplus 5A_{2u} \oplus 10E_u \oplus 18F_{1u} \oplus 16F_{2u} \end{aligned}$$

Of these, 55 modes are inactive, 25 are Raman-active ($3A_{1g}\oplus 8E_g \oplus 14F_{2g}$), and 17 are IR-active (F_{1u} symmetry; one additional F_{1u} mode corresponds to translations).

A. IR Spectrum and TO−LO Splitting. The simulated IR spectrum of almandine is reported in Table 2, where experimental data collected by Hofmeister and Chopelas[7] (HC in the following) are also included. The full set of 17 T_{1u} TO and LO observed modes has been identified and assigned to the corresponding computed values. Two steps are required to build up the table: (a) identify the simulated-to-experimental correspondence and (b) identify (if possible) the TO-to-LO correspondence (LO−TO splitting or shift).

Regarding point b, in the experimental works of Hofmeister et al.,[7,22,23] a pairing scheme was proposed according to which LO wavenumbers are usually higher than the TO values (the LO−TO shift is positive) in such a way that the corresponding TO and LO modes occupy the same position in the respective sets ordered by increasing wavenumber. In some cases, however, inversions appear: as the LO−TO shift is related to the strength of the oscillator, inversions are observed[7,22,23] when a low-intensity TO mode is just above (in sequential order) and close (on the wavenumber scale) to a TO mode with high intensity.

Two inversions are indeed reported in the HC[7] set of data, namely, those involving the 882 and 461 cm^{-1} LO modes; see Table 2.

An LO−TO correspondence based only on these arguments does not appear to be fully satisfactory, however. Simulation can help to identify alternative criteria for the LO−TO correspondence. As discussed in a previous work by some of the present authors,[5] the TO−LO correspondence is possible without ambiguity in cases where a single mode exists for each irreducible representation of the group at the Γ point; in all other cases, the two sets of modes (LO and TO) are independent, resulting from independent diagonalizations of the W and $W + W^{\mathrm{NA}}$ dynamical matrices, where W^{NA} is the nonanalytical correction (see ref 24, sections 5, 10, 34, and 35, and ref 25.)

To establish a similarity between TO and LO modes, an overlap criterion was introduced that consists of evaluating the (nonsymmetric) overlap matrix between TO and LO modes. The TO−LO correspondence is then based on the obvious observation that very similar modes overlap to a large extent whereas dissimilar modes do not. In Table 2, the TO−LO overlap (normalized to 100) is, in most cases, greater than or equal to 70; in these cases, the TO−LO correspondence is clearly defined. In two cases, however, the largest overlap is only 49 and 55. These two cases are, as expected, characterized by a large LO−TO shift: the large W^{NA} off-diagonal contribution brings about a large mixing with other modes. The corresponding LO−TO splitting is larger than 100 cm^{-1}, whereas in all other cases, it is smaller than 30 cm^{-1}. These two peaks are characterized by very high intensity, in agreement with Hofmeister et al.'s analysis.

According to the overlap criterion, five modes (in bold in Table 2) have been reassigned. Three additional inversions (with respect to Hofmeister et al.'s classification) appear then in the table.

The accuracy of the computed wavenumbers can be summarized in terms of a few statistical indices. The mean absolute difference, $|\bar{\Delta}| = 6.3$ and 5.2 cm^{-1}, and the mean difference, $\bar{\Delta} = 1.9$ and -0.1 cm^{-1}, for the TO and LO sets, respectively, indicate that only minor discrepancies exist between computed

and experimental wavenumbers and that systematic errors are nearly completely absent. Only in one case (in the low part of the spectrum; the mode involves Fe^{2+} in the dodecahedral site) does the difference exceed 30 cm^{-1}; a strong anisotropic component, suggested by X-ray diffraction and Mössbauer spectroscopy experiments[20,21] and not taken into account by our harmonic model, might be responsible for a fraction of the difference. In only three other cases is the difference greater than 10 cm^{-1}.

A more direct comparison of the calculation with the primary experimental data is possible by computing the reflectivity spectrum, $R(\nu)$, which, for normal incidence, is defined as[26]

$$R(\nu) = \left|\frac{\sqrt{\epsilon(\nu)} - 1}{\sqrt{\epsilon(\nu)} + 1}\right|^2 \quad (2)$$

The complex dielectric function of the crystalline system is defined as

$$\epsilon(\nu) = \epsilon_\infty + \sum_j \frac{f_j \nu_j^2}{\nu_j^2 - \nu^2 - i\nu\gamma_j} \quad (3)$$

where ν_j, f_j, and γ_j are the TO peak positions, their oscillator strengths, and their damping values, respectively; the value $\epsilon_\infty = 2.77$ was used for almandine.

Using a microscopic approach to the calculation of the dieletric function, for an isotropic system, one can write[24,27,28]

$$\epsilon(\nu) = \epsilon_\infty + \frac{4\pi}{\Omega}\sum_j \frac{\bar{Z}_j^2}{\nu_j^2 - \nu^2 - i\nu\gamma_j} \quad (4)$$

The strength of the jth oscillator of an isotropic crystal, given by

$$f_j = \frac{4\pi}{\Omega}\frac{\bar{Z}_j^2}{\nu_j^2} \quad (5)$$

is a value proportional to the mass-weighted effective mode Born charges $\bar{Z}_j^2$ and to the volume of the cell Ω.

Despite large absolute differences, the computed and experimental oscillator strengths (Table 2) show comparable trends. There are many possible explanations for the quantitative differences: On the simulation side, oscillator strengths based on the Born charges are computed assuming that the transient dipole moment varies linearly with the normal coordinate. This condition can sometimes be significantly violated. On the experimental side, oscillator strengths, TO wavenumbers, and damping values are simultaneously obtained by fitting the dielectric function of eq 3 with the experimental one derived from the experimental reflectivity spectrum (see eq 2). Large correlations among the fitting parameters can exist, as confirmed by the fact that large differences between experimental and computed oscillator strengths correspond to large discrepancies between calculated and observed wavenumbers (see Table 2). Nevertheless, $R(\nu)_{exp}$[7] and $R(\nu)_{calc}$ are in good agreement along the entire spectrum, with the exception of the low-frequency region (below 150 cm^{-1}), as shown in Figure 1.

As regards the damping values, γ_j, which are not directly accessible to simulation at the moment, a constant value (γ_j = 8 cm^{-1}) was used. The use of the experimental γ_j[7] values provides essentially the same simulated spectrum, because the damping values affect the heights of peaks but not their positions and widths.[26]

B. Raman Spectrum. In Table 3, our Raman results are compared to the four most recent sets of measured data [Hofmeister and Chopelas[7] (HC), Kolesov and Geiger[8] (KG), Makreski et al.[10] (MA), Calligaro et al.[9] (CA)] collected in 1998−2005.

The HC and KG data were recorded with the polarization dependence of the peaks detected in a way that allowed

TABLE 2: Calculated and Experimental[7] IR TO and LO Modes (F_{1u} Symmetry) of Almandine $Fe_3Al_2Si_3O_{12}$ and Their Calculated Strengths[a]

IR TO modes						IR LO modes			LO−TO	
ν_{calc}	ν_{exp}	$\Delta\nu$[b]	f_{calc}	f_{exp}	Δf[c] (%)	ν_{calc}	ν_{exp}	$\Delta\nu$	$\delta\nu$[d]	S[e]
103.8	111.5	−7.7	2.76	0.9	67.3	105.1	115	−9.9	1.3	78
107.0	137.5	−30.5	3.53	1.9	46.2	137.4	147	−9.6	30.4	74
160.2	157.6	2.6	0.069	0.18	−160.5	161.3	160	1.3	1.1	98
195.4	196.3	−0.9	0.58	0.55	5.9	203.7	205	−1.3	8.3	95
238.0	236	2.0	0.27	0.225	17.9	243.0	246	−3.0	5.0	97
318.2	318.1	0.1	0.37	0.21	43.2	323.4	322	1.4	5.2	96
348.4	344.6	3.8	0.31	0.12	60.6	352.6	347	5.6	4.2	94
374.1	376.2	−2.1	0.75	0.7	6.2	390.5	396	−5.5	16.4	87
413.2	412	1.2	0.028	0.025	11.8	413.8	422	−8.2	0.6	99
449.5	448	1.5	1.51	1.55	−2.9	604.0	**597.2**	**6.8**	154.5	49
466.3	467.7	−1.4	0.21	0.28	−34.9	464.1	461	3.1	−2.2	92
522.3	525.1	−2.8	0.028	0.008	71.4	519.1	**518**	**1.1**	−3.2	92
563.0	561.1	1.9	0.14	0.16	−10.9	541.1	**534.4**	**6.7**	−21.9	71
636.7	634.5	2.2	0.024	0.011	54.7	643.6	638	5.6	6.9	93
873.0	865.3	7.7	0.43	0.6	−39.8	1057.4	**1038**	**19.4**	184.4	55
896.9	889.2	7.7	0.11	0.1	10.4	890.5	882	8.5	−6.4	81
964.6	952.3	12.3	0.17	0.18	−8.7	933.3	**923**	**10.3**	−31.3	69
	$\lvert\bar{\Delta}\rvert$[f]	5.2					$\lvert\bar{\Delta}\rvert$	6.3		
	$\bar{\Delta}$	−0.1					$\bar{\Delta}$	1.9		
	$\lvert\Delta_{max}\rvert$	30.5					$\lvert\Delta_{max}\rvert$	19.4		

[a] Frequencies and differences in cm^{-1}. [b] Difference between calculated and experimental data. [c] Percentage difference between calculated and experimental oscillator strengths. [d] Calculated LO−TO splitting. [e] Largest overlap (multiplied by 100) between the TO eigenvector identified by the row and the full set of LO eigenvectors. [f] Statistical indices explained in text.

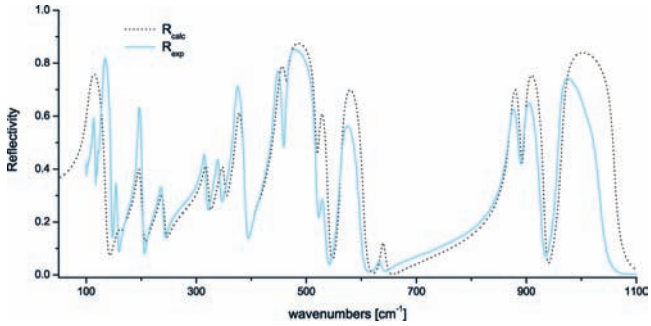

Figure 1. Experimental[7] and calculated (from the data of Table 2) reflectivity spectra of almandine. See text for details.

symmetry classification, whereas the other two sets were not classified by symmetry, and the positions of the data sets in the table were chosen simply on the basis of numerical proximity to the calculated wavenumbers.

Table 3 contains 31 rows instead of the expected 25. Extra entries correspond to observed wavenumbers that do not have a corresponding computed value in a relatively large range (rows 5, 9, 13, 19, 20, and 28) and to calculated peaks for which an experimental counterpart cannot be identified on the basis of the same criterion (rows 6, 15, and 23).

HC[7] reported a complete set of 25 peaks. It was not possible, however, to establish a one-to-one correspondence between all of the computed and experimental wavenumbers. Indeed, four of six extra experimental peaks in Table 3 (rows 9, 13, 19, and 20) appear in the HC set. The two E_g peaks at 421 and 910 cm^{-1} are 46 and 48 cm^{-1} higher than the closest calculated peaks with the same symmetry (at 375 and 862 cm^{-1}, respectively); the two F_{2g} modes at 239 and 293 cm^{-1} are about 20 cm^{-1} from the closest computed wavenumbers (at 272 and 311 cm^{-1}, respectively). The position of peak 20 (at 293 cm^{-1}) was reported to be uncertain because of the breadth and weakness of the band.[7] This last peak cannot be related to the computed absorption at 297 cm^{-1} (extra row 6) because its symmetry is E_g instead of F_{2g}, so that a wrong symmetry attribution of the experimental mode could be invoked. A symmetry attribution problem might be invoked also for the extra experimental mode in row 13 (F_{2g} symmetry), which is exactly at the same frequency as the A_g peak in row 3.

For the remaining 21 peaks, the correspondence between computed and observed values can be established unambiguously.

KG[8] provide 20 of the 25 peaks. Only the E_g peak at 255 cm^{-1} (line 5) has no computed counterpart: it is more than 40 cm^{-1} lower than the closest calculated peak with the same symmetry (297 cm^{-1}); this peak is not included in any other set, although a peak at about the same wavenumber (266 cm^{-1}) was reported in previous work by Moore et al.[29] This peak has low intensity; an analogous weak mode was observed in the

TABLE 3: Observed and Calculated Raman-Active Modes of Almandine (cm^{-1})[a,b]

	this work	HC		KG		MA		CA	
	ν	ν	$\Delta\nu$	ν	$\Delta\nu$	ν	$\Delta\nu$	ν	$\Delta\nu$
				A_g					
1	334.0	347	−13.0	342	−8.0	347	−13	–	–
2	555.3	553	2.3	556	−0.7	559	−3.7	557	−1.7
3	918.4	910	8.4	916	2.4	921	−2.6	917	1.4
				E_g					
4	164.2	163	1.2	167	−2.8	–	–	168	−3.8
5	–	–	–	256	–	–	–	–	–
6	297.0	–	–	–	–	–	–	–	–
7	321.8	326	−4.2	323	−1.2	318	3.8	317	4.8
8	374.5	368	6.5	370	4.5	–	–	–	–
9	–	421	–	–	–	–	–	–	–
10	529.2	521	8.2	–	–	–	–	–	–
11	597.5	593	4.5	596	1.5	–	–	–	–
12	862.6	–	–	–	–	–	–	–	–
13	–	910	–	–	–	–	–	–	–
14	938.5	920	18.5	930	8.5	–	–	–	–
				F_{2g}					
15	99.4	–	–	–	–	–	–	–	–
16	153.2	166	−12.8	170	−16.8	–	–	–	–
17	173.9	198	−24.1	171	2.9	–	–	–	–
18	217.9	212	5.9	216	1.9	–	–	–	–
19	–	239	–	–	–	240	–	–	–
20	–	293	–	–	–	–	–	–	–
21	310.8	312	−1.2	314	−3.2	–	–	–	–
22	344.1	355	−10.9	–	–	349	−4.9	347	−2.9
23	367.3	–	–	–	–	372	−4.7	370	−2.7
24	474.3	474	0.3	475	−0.7	481	−6.7	–	–
25	501.6	498	3.6	500	1.6	502	−0.4	501	0.6
26	586.2	576	10.2	581	5.2	586	0.2	–	–
27	635.9	628	7.9	630	5.9	636	−0.1	625	10.9
28	–	–	–	–	–	687	–	683	–
29	864.6	862	2.6	863	1.6	863	1.6	862	2.6
30	900.2	892	8.2	897	3.2	–	–	–	–
31	1045.4	1032	13.4	1038	7.4	1044	1.4	1042	3.4

[a] Experimental data from Hofmeister and Chopelas[7] (HC), Kolesov and Geiger[8] (KG), Makreski et al.[10] (MA), and Calligaro et al.[9] (CA). [b] Symbols as in Table 2.

TABLE 4: Statistics of Raman-Active Modes of Almandine (cm^{-1})[a,b]

		HC	KG	MA	CA
this work	M	21	19	12	10
	$\lvert\bar{\Delta}\rvert$	8.0	4.2	3.6	3.5
	$\bar{\Delta}$	1.6	0.7	−2.4	1.3
	$\lvert\Delta_{max}\rvert$	24.1	16.8	6.7	10.9
HC	M		19	12	9
	$\lvert\bar{\Delta}\rvert$		5.0	6.2	5.4
	$\bar{\Delta}$		−1.3	−3.8	−1.0
	$\lvert\Delta_{max}\rvert$		27.0	12	10
KG	M			10	8
	$\lvert\bar{\Delta}\rvert$			4.3	2.5
	$\bar{\Delta}$			−3.3	0.5
	$\lvert\Delta_{max}\rvert$			6	6
MA	M				10
	$\lvert\bar{\Delta}\rvert$				3.0
	$\bar{\Delta}$				3.0
	$\lvert\Delta_{max}\rvert$				11

[a] Experimental data from Hofmeister and Chopelas[7] (HC), Kolesov and Geiger[8] (KG), Makreski et al.[10] (MA), and Calligaro et al.[9] (CA). [b] Symbols as in Table 2.

E_{2g} Raman spectra of spessartine at 269 cm^{-1} and in that of grossular at 320 cm^{-1}.[8]

The remaining two sets, MA and CA, contain 14 and 11 peaks, respectively. The extra F_{2g} peak at 687 cm^{-1} (MA) or 683 cm^{-1} (CA) (line 28), not observed by HC and KG, is very far from the nearest calculated mode at 636 cm^{-1}; the "twin" structure of this peak is not observed in the calculated spectrum or in any other experimental sets. The other extra peak in MA (line 19) is also reported by HC and not by other authors. In summary, three of the six "extra" experimental peaks are proposed by HC only, one by KG only, one by HC and MA, and one by MA and CA.

The following observations can help in understanding the origin of the extra peaks reported in Table 3:

All computed wavenumbers are affected by about the same inaccuracy, irrespective of their position in the spectrum and of their intensity, because all of them are calculated by the same algorithm. On the contrary, the attribution of each experimental mode can be difficult for several different reasons: low intensity, background, overtones, peak superposition, and others.

On the basis of these considerations, the six extra peaks of the experimental sets can confidently be considered spurious attributions rather than the result of inaccuracy in the simulation. For instance, extra peak 5 in the KG set (256 cm^{-1}) is probably a combined mode resulting from modes 15 and 16 (99 + 153 = 252 cm^{-1}; the symmetry is compatible, as resulting from the direct product $F_{2g}\otimes F_{2g} = A_{1g}\oplus E_g\oplus F_{1g}\oplus F_{2g}$).[26]

On the other hand, the three extra calculated peaks with no experimental counterpart (rows 6, 15, and 23) can be supposed to have low intensity (at the moment, we are unable to compute Raman intensities).

Additional information about the discrepancies between the various sets of experimental data and between calculation and experiment is provided by the statistical indices given in Table 4. Obviously, extra peaks are not included in the statistics. The mean absolute and largest wavenumber differences ($\lvert\bar{\Delta}\rvert$ = 5.0 cm^{-1} and $\lvert\Delta_{max}\rvert$ = 27.0 cm^{-1}) between the two almost complete sets (HC[7] and KG[8]) show a few systematic discrepancies and a good agreement for the common set of 19 peaks. When the comparison is extended to the other sets of experimental data, $\lvert\bar{\Delta}\rvert$ ranges from 3 and 7 cm^{-1}, and $\lvert\Delta_{max}\rvert$ never exceeds 12 cm^{-1} (the number of common peaks is in some cases quite small, however). The agreement between the computed and experimental data is quite satisfactory, with $\lvert\bar{\Delta}\rvert$ and $\lvert\Delta_{max}\rvert$ ranging from 3.5 to 6.7 cm^{-1} and from 3 to 24 cm^{-1}, respectively. Experimental limitations might be responsible for the largest wavenumber differences, $\lvert\Delta_{max}\rvert$ = 24.1 and 16.8 cm^{-1} in comparison with the HC[7] and KG[8] sets, respectively, both in the low-frequency region (lines 16 and 15 of Table 3). It is worth noticing that $\lvert\Delta_{max}\rvert$ = 27 cm^{-1} for a comparison of HC[7] and KG[8] (see Table 4).

C. Graphical Animation of Modes. Animations representing the 17 IR-active, 25 Raman-active, and 55 silent modes are available at the CRYSTAL Web site.[30] To make the animation as clear as possible, only a fraction of the unit cell is shown, containing one AlO_6 octahedron and the six SiO_4 tetrahedra linked to it. However, because Fe ions are involved in many modes, additional animations are provided for a larger fragment containing six Fe ions.

IV. Conclusions

The transverse and longitudinal optical IR and the Raman vibrational wavenumbers of end-member almandine have been calculated at an ab initio quantum-mechanical level and compared with available experimental data. The agreement is excellent for both IR and Raman spectra. IR intensities have also been computed and compared to the experimental oscillator strengths. The two sets of data show comparable trends. The reflectivity spectrum computed from the observed and calculated frequencies and oscillator strengths is also in excellent agreement.

The quality of the results is very similar to that obtained for other end-member garnets; for example, for the IR TO vibrations of grossular, andradite, and pyrope $\lvert\bar{\Delta}\rvert$ is 5.8, 6.9, and 6.6 cm^{-1}, respectively.

Calculation always provides the full set of wavenumbers and permits the integration of the experimental set with those wavenumbers that are not easily detected experimentally because of low intensity.

The present study confirms that simulation is currently able to describe structural and vibrational properties of large unit cell systems such as garnets and that simulation can therefore be used as a complementary tool to experimental techniques.

Acknowledgment. The authors are grateful to Prof. A. Hofmeister for the almandine reflectivity experimental spectrum. This work was supported by the Italian MIUR through a Cofin2007 project.

References and Notes

(1) Deer, W.; Howie, R.; Zussman, J. *An Introduction to the Rock Forming Minerals*; John Wiley: New York, 1992.

(2) Dovesi, R.; Saunders, V. R.; Roetti, C.; Orlando, R.; Zicovich-Wilson, C. M.; Pascale, F.; Doll, K.; Harrison, N. M.; Civalleri, B.; Bush, I. J.; D'Arco, P.; Llunell, M. *Crystal06 User's Manual*; Università di Torino, Torino, Italy, 2006.

(3) Pascale, F.; Zicovich-Wilson, C. M.; Orlando, R.; Roetti, C.; Ugliengo, P.; Dovesi, R. *J. Phys. Chem. B* **2005**, *109*, 6146–6152.

(4) Pascale, F.; Catti, M.; Damin, A.; Orlando, R.; Saunders, V. R.; Dovesi, R. *J. Phys. Chem. B* **2005**, *109*, 18522–18527.

(5) Zicovich-Wilson, C. M.; Torres, J.; Pascale, F.; Valenzano, L.; Orlando, R.; Dovesi, R. *J. Comput. Chem.* **2008**, *29*, 2268–2278.

(6) Valenzano, L.; Meyer, A.; Demichelis, R.; Civalleri, B.; Dovesi, R. *Phys. Chem. Miner.* **2009**, *36*, 415.

(7) Hofmeister, A. M.; Chopelas, A. *Phys. Chem. Miner.* **1991**, *17*, 503–526.

(8) Kolesov, B.; Geiger, C. A. *Phys. Chem. Miner.* **1998**, *25*, 142–151.

(9) Calligaro, T.; Colinart, S.; Poirot, J.; Sudres, C. *Nucl. Instrum. Methods Phys. Res. B* **2002**, *109*, 320–327.

(10) Makreski, P.; Jovanovski, G.; Stojanceska, S. *J. Mol. Struct. (THEOCHEM)* **2005**, *744−747*, 79–92.

(11) Gramaccioli, C. M.; Pilati, T. *J. Phys. Chem. A* **2003**, *107*, 4360.
(12) Becke, A. D. *J. Chem. Phys.* **1993**, *98*, 5648–5652.
(13) Koch, W.; Holthausen, M. C. *A Chemist's Guide to Density Functional Theory*; Wiley-VCH Verlag GmbH: Weinheim, Germany, 2000.
(14) Zicovich-Wilson, C. M.; Pascale, F.; Roetti, C.; Saunders, V. R.; Orlando, R.; Dovesi, R. *J. Comput. Chem.* **2004**, *25*, 1873–1881.
(15) Prencipe, M.; Pascale, F.; Zicovich-Wilson, C. M.; Saunders, V. R.; Orlando, R.; Dovesi, R. *Phys. Chem. Miner.* **2004**, *31*, 559–564.
(16) Orlando, R.; Torres, F. J.; Pascale, F.; Ugliengo, P.; Zicovich-Wilson, C. M.; Dovesi, R. *J. Phys. Chem. B* **2006**, *110*, 692–701.
(17) List of inputs/outputs - GARNETS: frequency calculations; available at www.theochem.unito.it/garnets.
(18) Pascale, F.; Zicovich-Wilson, C. M.; Gejo, F. L.; Civalleri, B.; Orlando, R.; Dovesi, R. *J. Comput. Chem.* **2004**, *25*, 888–897.
(19) Novak, G. A.; Gibbs, G. V. *Am. Mineral.* **1971**, *56*, 791–825.
(20) Armbruster, T.; Geiger, C. A.; Lager, G. A. *Am. Mineral.* **1992**, *77*, 512.
(21) Geiger, C. A.; Armbruster, T.; Lager, G. A.; Jiang, K.; Lottermoser, W.; Amthauer, G. *Phys. Chem. Miner.* **1992**, *19*, 121.
(22) Hofmeister, A. M.; Fagan, T. J.; Campbell, K. M.; Schaal, R. B. *Am. Mineral.* **1996**, *81*, 418–428.
(23) McAloon, B. P.; Hofmeister, A. M. *Am. Mineral.* **1995**, *80*, 1145–1156.
(24) Born, M.; Huang, K. *Dynamical Theory of Crystal Lattices*; Oxford University Press: Oxford, U.K., 1954.
(25) Umari, P.; Pasquarello, A.; Corso, A. D. *Phys. Rev. B* **2001**, *63*, 094305.
(26) Decius, J.; Hexter, R. *Molecular Vibrations in Crystals*; McGraw-Hill: New York, 1977.
(27) X. Gonze, C. L. *Phys. Rev. B* **1997**, *55*, 10355.
(28) Kleinmann, D. A.; Spitzer, W. G. *Phys. Rev.* **1962**, *125*, 16.
(29) Moore, R.; White, W. B. *Am. Mineral.* **1971**, *56*, 54–71.
(30) Animations of almandine vibration modes; available at http:/www.crystal.unito.it/vibs/garnets/almandine.

JP901993E